NANO LETTERS

Letter

pubs.acs.org/NanoLett

Control of Emergent Properties at a Correlated Oxide Interface with Graphene

You Zhou,*[,†] Jungwon Park,[†] Jian Shi,[†] Manish Chhowalla,[‡] Hyesung Park,[§] David A. Weitz,[†,∥] and Shriram Ramanathan[†]

[†]School of Engineering and Applied Sciences, Harvard University, Cambridge, Massachusetts 02138, United States

[‡]Department of Materials Science, Rutgers, the State University of New Jersey, Piscataway, New Jersey 08854, United States

[§]School of Energy and Chemical Engineering, Ulsan National Institute of Science and Technology, Ulsan 689-798, South Korea

[∥]Department of Physics, Harvard University, Cambridge, Massachusetts 02138, United States

Supporting Information

ABSTRACT: Electrolyte gating of complex oxides enables investigation of electronic phase boundaries and collective response to strong electric fields. The origin of large conductance modulations and associated emergent properties in such field effect structures is a matter of intense study due to competing contributions from electrostatic (charge accumulation) and electrochemical (crystal chemistry changes) effects. Vanadium dioxide (VO_2) is a prototypical correlated insulator that shows an insulator-to-metal transition at ~67 °C and recent studies have noted a vast range of electronic effects in electric double-layer transistors (EDLT). In this study, we demonstrate that the response of electrolyte gated VO_2 devices can be deterministically controlled by inserting a monolayer of graphene at the oxide−electrolyte interface. Several electrolytes as well as dopants (such as lithium ions and protons) were employed in EDL transistors to show that graphene serves as an inert barrier that successfully protects the oxide surface from chemical reactions. This monolayer interface has a striking effect on resistance modulation in the vanadium dioxide transistor channel up to several orders of magnitude and enables retention of the insulating phase. The studies allow new insights into the response of correlated insulators in EDLTs and inform design of correlated oxide−2D heterostructures for electronics and sensors.

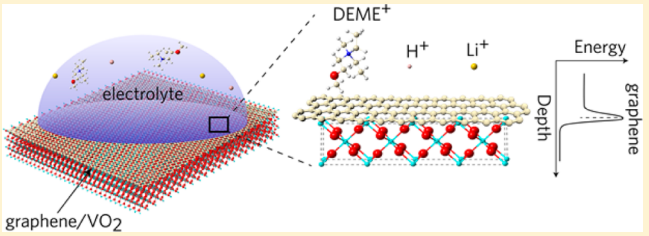

KEYWORDS: *Electrochemical doping, graphene, vanadium dioxide, ion selectivity, metal−insulator transition, electric double layer transistor*

Controlling charge carriers via electric fields in transition metal oxides has been one of the major efforts in the development of oxide-based functional devices and understanding physical behavior of correlated electron systems. Beyond the simple linear tuning of the conductivity as a function of free carrier concentration, controlling the carrier concentration in such oxides can lead to emergent phenomena such as superconductivity, magnetic ordering, and metal−insulator transitions.[1−3] Electrolyte gating utilizes the electric-double layer (EDL) that forms at the liquid−solid interfaces to induce large carrier accumulation at the channel surface and enables one to reversibly probe emergent physicochemical properties in correlated oxides.[3−7] The choice of liquids depends on the temperature range of electronic measurements and the capacitance density required for modifying the properties of the oxide. Although many ionic liquids employed in such studies have wide electrochemical windows up to ±4 V, these parameters were measured with respect to inert electrodes such as platinum, tungsten, or glassy carbon[8−10] and may not be directly applicable to complex oxide interfaces. In fact, the transition metal cations in correlated oxides usually can take on multiple valence states and many of the oxides have polar surfaces, which makes them prone to react with ions (through charge transfer) in an electrolyte under a large electric field. Thus, understanding the importance of electrochemistry and the further methods to control the interfacial charge transfer and the related electronic conductivity at interfaces are important topics for fundamental research and have implications for the design of field effect devices with high carrier density systems in a broader setting.

In this study, we report a new approach to control the electrochemical reactions between a model correlated oxide, VO_2, and various electrolytes in an EDL transistor geometry by utilizing a monolayer of graphene at the interface that is chemically protective. Although graphene is atomically thin, it is a remarkable ionic insulator with a small ionic conductance depending on the ion species.[11] This is largely due to the strong C−C bond with bonding energy of 4.9 eV and small geometric

Received: October 30, 2014
Revised: January 25, 2015
Published: February 5, 2015

DOI: 10.1021/nl504170d
Nano Lett. 2015, 15, 1627−1634

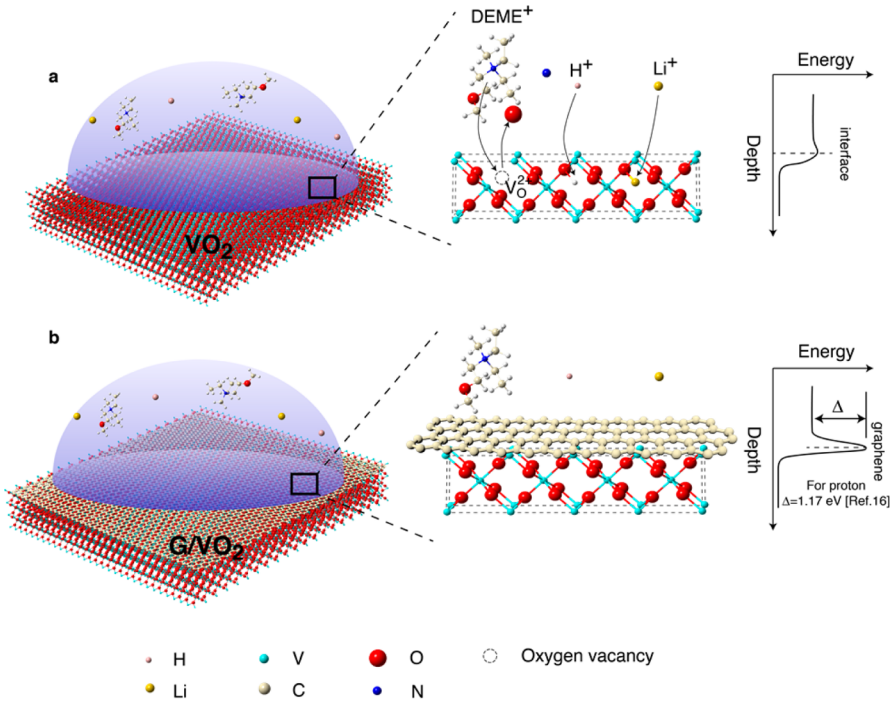

Figure 1. (a) During electrolyte gating, electron donors such as oxygen vacancies, hydrogen, and lithium interstitials could be created in VO_2 by electrochemical processes, which modulates the conductivity of VO_2 and alter the phase boundary for insulator−metal transitions. The energy profile of ions under a driving force of positive gate bias is shown. (b) A monolayer of graphene is interfaced between the electrolyte and VO_2 to protect the oxide surface. The monolayer of graphene acts as a diffusional barrier for ions with a barrier height of a few electron volts depending on the ionic species (ref 16), which can drastically suppress the channel response to external gate bias.

pores.[12] Such property has led to unique applications such as encasing liquids for wet transmission electron microscopy,[13] selective molecular sieving,[14] and water desalination.[15] In the present study, the ionic impermeability of graphene allows us to isolate the ions in the electrolyte from a reactive oxide surface and examine the mechanism of electrolyte gating. Figure 1a shows the possible electrochemical processes that could happen under bias during electrolyte gating. Depending on the ionic species in the electrolytes, different electron donors such as oxygen vacancies, hydrogen, and lithium interstitials could be created or incorporated in VO_2. The extra carriers could induce a phase transition in VO_2 through electron−electron or electron lattice interactions, leading to a sharp decrease in the channel resistivity, often referred to as emergent behavior. By transferring a monolayer of graphene onto a correlated oxide surface, we introduce an energy barrier for ionic transport as shown in Figure 1b. The energy barrier for hydrogen ion to penetrate a monolayer of graphene has been reported to be on the order of ∼1 eV,[16] and one would expect even larger energy barriers for ions with larger ionic radii. Therefore, the oxide underneath is protected from electrochemical reactions leading to crystal chemistry changes and the conductance modulation can be controlled. On the basis of the above design, gating experiments have been carried out on graphene-coated EDL transistors using various kinds of electrolytes as well with different ions such as H^+ and Li^+ and it is shown that the ion selectivity of graphene can lead to strikingly different electric field response. The conductance modulation arising from emergent phases and electrochemical instability is completely suppressed for ionic liquid gating when graphene is present. The methods could be readily transferable to a broad range of complex oxides to examine the nature of the EDL gating and also to protect oxide surfaces especially in reactive environments such as biological media. The ion selectivity of graphene combined with the response of correlated oxides may point to novel applications such as active ion sensors/filters, artificial ion channels, and quantum point contacts.

VO_2 EDLT devices were fabricated on *c*-plane sapphire. Graphene was synthesized by chemical vapor deposition on a copper foil and transferred onto the fabricated device using poly(methyl methacrylate) (PMMA) supported direct transfer method as shown in Figure 2a. Figure 2b shows an optical image of a typical G/VO_2 device with a drop of ionic liquid. The probe acting as gate electrode is not shown in the image. The magnified image shows the channel region without ionic liquid. The liquid covers the entire channel region in both G/VO_2 and bare VO_2 cases. As-transferred graphene covers the device conformally as indicated by AFM studies and is mechanically stable throughout the experiments (Supporting Information Figure S1 and S2). SEM image of the devices shows that there is no pinhole at the channel surface (Supporting Information Figure S3). The sheet resistance of VO_2 channel decreases sharply around its phase transition temperature for both pristine and graphene-coated VO_2, indicating that the chemical and physical behavior of VO_2 film is not perturbed by graphene (see Supporting Information Figure S4).

Previous studies on electrolyte gating of complex oxides have primarily used room-temperature ionic-liquids and are suited for probing vanadium dioxide.[7,17−22] Therefore, we first performed gating experiments using the ionic liquid, *N*,*N*-diethyl-*N*-(2-methoxyethyl)-*N*-methylammonium bis-(trifluoromethylsulfonyl-imide (DEME-TFSI), on both pristine and graphene-protected VO_2 EDLT devices. Figure 3 shows the temporal response of the channel resistance of VO_2 and VO_2/graphene EDLTs under different gate voltages. For a bare

DOI: 10.1021/nl504170d
Nano Lett. 2015, 15, 1627−1634

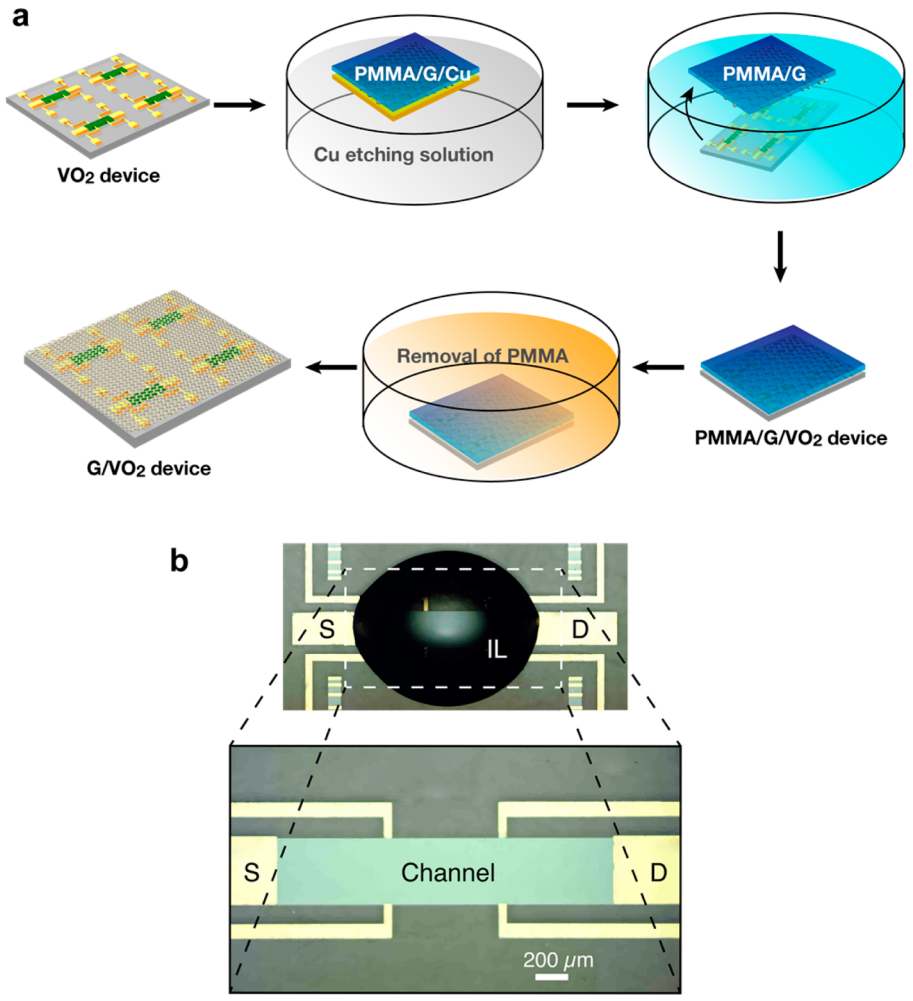

Figure 2. (a) Schematic of experimental scheme to transfer CVD-grown graphene from Cu foils onto fabricated VO_2 electric double layer transistor devices. (b) Optical image of a graphene-coated VO_2 device with a drop of ionic liquid on top. The magnified image shows the channel region without the ionic liquid.

VO_2 device (i.e., with no graphene overlayer), the channel resistance starts to decrease at a threshold gate bias between +1.5 and +2 V. At larger bias, the resistance modulation happens at a time scale of a few hours and the largest resistance modulation is about 2 orders of magnitude at 2.5 V. The conductance modulation is nonvolatile, namely, the channel resistance remains at this reduced value for days at ambient conditions. In contrast, the channel resistance of the graphene-coated EDLT devices is constant for all applied voltages.

Two scenarios are possible in electrolyte gating. If ions only accumulate and form an EDL at the solid/liquid interface, the extra carriers are induced electrostatically. If there is interfacial electron transfer between the ions in the solution and channel, electrochemical effects could lead to resistance modulation by creating defects (and corresponding charge compensation). In the electrostatic picture, if we assume to first order that the carrier mobility is not strongly changed by the carrier concentration, the electrostatic modulation of channel sheet conductivity $\Delta\sigma$ is given by $\Delta\sigma = q\mu_G\Delta n_G + q\mu_{VO_2}\Delta n_{VO_2}$ where q is the electron charge, μ_G and μ_{VO_2} are the carrier mobility of graphene and vanadium dioxide, respectively, and Δn_G and Δn_{VO_2} are the change in the sheet carrier concentration in graphene and VO_2, respectively. The carrier concentration in graphene is $\sim 10^{11}$ cm^{-2} as measured from Hall measurements, and the areal carrier density of VO_2 is $\sim 10^{13}$ cm^{-2}. Note that there would be charge transfer between VO_2 and graphene because of the slight work function difference as they are in contact suggested by AFM but this would not influence the gating results in electrostatic picture because of metal gate electrode determines the Fermi level positioning of semiconductors at zero gate bias and the work function values of graphene, VO_2, and gold-coated tungsten gate electrode are similar.[23,24]

We can then analyze the screening effect of graphene and possible effect of air gap, assuming uniform electric field in-plane. The relation between the electric potential $\Phi(z)$ and net charge density $\rho(z)$ across the EDL and channel can be determined by the Poisson equation

$$\nabla^2\Phi(z) = -\frac{1}{\varepsilon_r\varepsilon_0}\rho(z) \quad (1)$$

, where $\rho(z)$ is a function of $\Phi(z)$. Ionic liquid and air gap can be modeled as parallel capacitor with zero net charge density inside, so electric field is a constant within them. For graphene and VO_2, eq 1 can be linearized by taking the first term in the Taylor expansion of $\rho(z)$, which results in an exponential decay of the potential $\Phi(z) = \Phi_0 e^{-z/L_D}$ in both materials, where L_D is the screening length of the material. The screening length of

DOI: 10.1021/nl504170d
Nano Lett. 2015, 15, 1627−1634

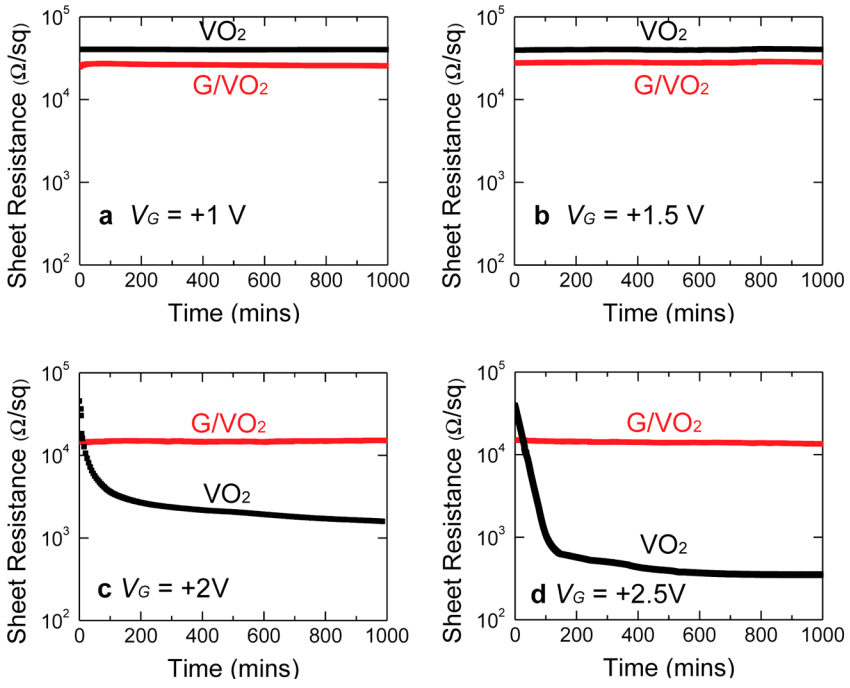

Figure 3. Time-dependent modulation of channel resistance of bare VO_2 and graphene-coated VO_2 under a constant gate voltage of (a) +1 V, (b) +1.5 V, (c) +2 V, (d) +2.5 V, respectively. Under a gate bias larger than +1.5 V, the channel conductance of a bare VO_2 device increases and reaches equilibrium after tens of minutes, while the conductance of graphene-coated VO_2 device remains unchanged for over a thousand minutes under all applied bias.

graphene is reported to be ~1 nm[25−28] while that of VO_2 can be estimated from $L_D = (\varepsilon_r\varepsilon_0 k_B T/q^2 n)^{1/2}$, where n is the free carrier density of VO_2.

Figure 4a shows the electric displacement field D across the ionic liquid and graphene protected VO_2, where D_0 is the electric displacement field right at the EDL. As a comparison, the electric displacement field in the bare VO_2 case is plotted in Figure 4b.

Note that D_0 is different in these two cases. To determine D_0, we use the boundary condition that the same voltage (V_G) is applied across the ionic liquid and channel, that is, $\int E dz = V_G$, where E is the electric field determined by $\varepsilon_r\varepsilon_0 E = D$. The total increase in the 2D free carrier density in each material can be then determined from Gauss's law. If we let $\Delta n = \Delta n_0$ in the bare VO_2 case, the increase in the carrier density will be $\Delta n_G = 0.31\Delta n_0$ and $\Delta n_{VO_2} = 0.76\Delta n_0$ for graphene and VO_2, respectively, in the G/VO_2 case. As a result, we would expect the increase in the VO_2 conductivity to be $\Delta G_{VO_2} = 0.76\Delta G_0$, where ΔG_0 is the increase in conductivity for bare VO_2. In addition, the conductivity of graphene will also increase as a result of increased carrier concentration. Thus, an increase in the channel conductance would have been observed in the experiments if there were primarily electrostatic modulation. If there is an air/vacuum gap between graphene and VO_2, but graphene can still transfer carriers to VO_2 as evidenced from electrical measurements, graphene would still screen the electric field. The electric displacement field would be constant across the gap as shown in Figure 4c. Assuming that the step height is 1 nm, the increase in the carrier concentration of VO_2 would be $\Delta n_{VO_2} = 0.25\Delta n_0$. Therefore, the G/VO_2 channel conductance modulation should still be observable as the bare VO_2 case. (The details of the analysis are included in the Supporting Information)

In sum, since the same magnitude of gate bias is applied and the estimated effective gate capacitance (including both the EDL in the electrolyte and the screening effects in graphene and VO_2) would not be much different for coated and uncoated VO_2 device, similar amount of carriers shall be induced in both cases. As a result, the channel resistance change in graphene-coated VO_2 will be on a similar order of magnitude with bare VO_2 EDLTs. However, our results show significant difference in the channel response of bare VO_2 and graphene-coated VO_2 devices. It gives rise to a strong indication that the cations in the ionic liquid need to be in contact with the reactive VO_2 surface to induce compositional changes in VO_2, which results in electrochemically induced conductance modulation. Likewise, it also confirms that the graphene layer is practically impermeable to the DEME cations or oxygen ions with large ionic radii, significantly inhibiting electrochemical effects in vanadium dioxide. Previous studies have demonstrated that graphene-based EDLTs on SiO_2 show bipolar modulation of the transport properties as a function of gate bias from EDL.[29] The charge modulation was only about 2× for gating with an ionic liquid, 1-butyl-3-methylimidazolium hexafluorophosphate (BmimPF6) at similar gate voltages as in the present study.

Confocal Raman spectroscopy was utilized to study possible chemical modification to graphene during the electrolyte gating process. Figure 5 compares the Raman spectra for both bare VO_2 and graphene-protected VO_2 devices before and after gating experiments. Figure 5a,b shows the Raman spectra from bare VO_2 and graphene-protected VO_2 devices before performing ionic liquid gating experiments. The peaks at 199, 228, 312, 394, 500, and 620 cm^{-1} matches well with the A_g modes of M1 phase of VO_2, while the B_g modes such as 339 and 422 cm^{-1} peaks can be seen as the shoulders of the higher intensity A_g peaks.[30,31] The peak positions of the Raman shift indicate that the VO_2 films are in the M1 phase. The similarity in VO_2 peak

DOI: 10.1021/nl504170d
Nano Lett. 2015, 15, 1627−1634

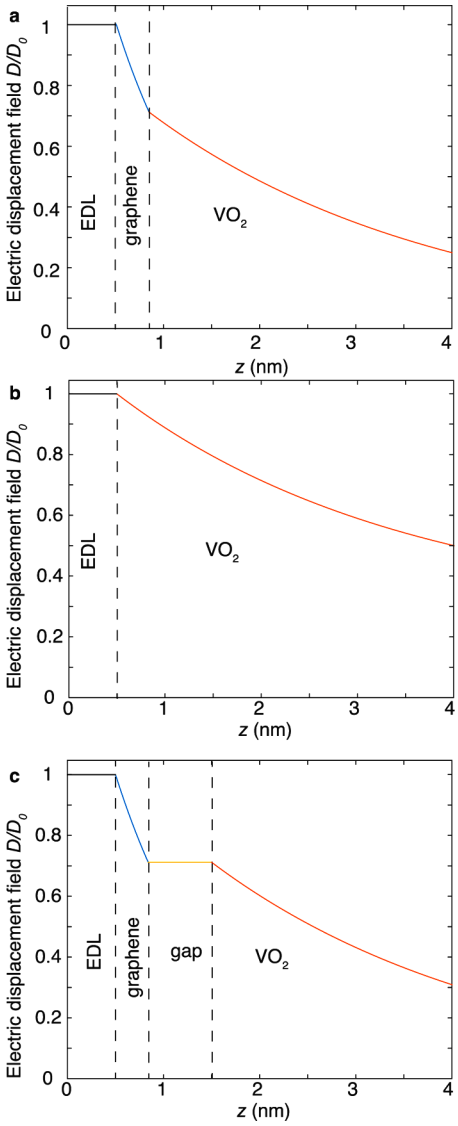

Figure 4. Electric displacement field profile of electrolyte gated (a) G/VO_2, (b) bare VO_2, and (c) G/VO_2 assuming that there is an air/vacuum gap formed between graphene and VO_2.

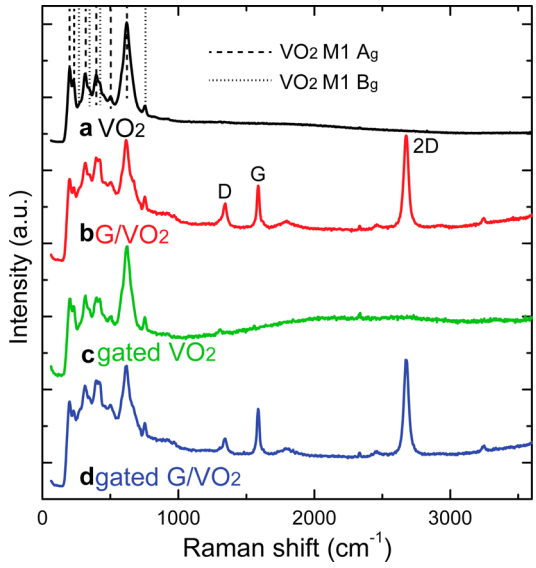

Figure 5. Raman spectra of (a) pristine bare VO_2, (b) pristine graphene-coated VO_2, (c) gated bare VO_2, (b) gated-graphene-coated VO_2, respectively. After gating, the Raman spectra of bare VO_2 are modified as a result of increased free carrier density, whereas there is no obvious change in the graphene-coated VO_2. The relative intensity and shape of Raman 2D, G, and D bands of graphene indicate that the graphene is intact during gating experiments.

position and shapes in Figure 5a,b indicate that VO_2 thin films remain intact during the graphene transfer process. The other peaks in Figure 5b correspond to the Raman signature of graphene. The G peak and 2D peak at ~1589 and ~2679 cm^{-1} in the measured spectra, correspond to the sp^2 C−C bond stretching and carbon ring breathing modes, respectively. The peak positions and their relative intensities indicate the graphene is indeed a monolayer.[32,33] We also observe another Raman peak at 1345 cm^{-1}, the D peak, arises from the presence of local defects in graphene but the intensity is relatively low. Those defects are possibly from local deformation of graphene during fabrication in ambient conditions. Overall, Raman measurements confirm the single layer graphene sheet is intact during device fabrication.[32,33]

We repeated the same Raman measurements for identical samples after gating under a constant gate bias of V_G = +2.5 V for 12 h with DEME-TFSI as an electrolyte. Then the ionic liquid was carefully removed by rinsing the samples in acetone, isopropanol, and DI water and blow-dried by N_2. The channel resistance is not influenced by the removal of the gating medium and is a constant over the course of the Raman experiments. The nonvolatility of the conductance modulation allows us to perform *ex situ* Raman studies, while also eliminating contributions from the ionic liquid. It is well-known that the characteristic Raman peaks of the monoclinic phase of VO_2 vanish and become a featureless dispersion upon the thermal transition into the metallic tetragonal phase. However, in our case, the VO_2 monoclinic phonon modes are still present after application of gate bias (Figure 5c), although the conductance is enhanced by about 2 orders of magnitude. Instead, the primary change seen is the appearance of a broad shape but not distinctive peaks in the large Raman shift range, which originates from the inelastic scattering of light by the extra free carriers induced by the gate electric field through electron−phonon coupling.[34,35] The Raman spectra of gated VO_2 samples are characterized by a combination of both insulating phonon modes and inelastic scattering from free carriers, while they do not show any Raman mode softening that could be caused by a structural change. The difference in the spectra between pristine and gated devices suggests the VO_2 films still contains the M1 phase. It is consistent with the scenario where electrochemical reactions take place at the interface between electrolyte and oxide and only a surface layer of the oxide is modified while the bulk of oxide remains intact due to the diffusional process.

In contrast to that of bare VO_2 device, the Raman spectra of graphene-protected VO_2 device are hardly influenced by external gate voltage. The Raman peak of gated graphene at 1345 cm^{-1} with similar peak shape and relative intensity after gating experiments indeed indicates that mechanical and chemical state of graphene is inert to applying the positive bias. Not only the characteristic VO_2 monoclinic and graphene Raman peaks but also the tail at large Raman shift remain intact, suggesting no extra carriers being induced by the gate bias, which is consistent with the electrical characterization results.

DOI: 10.1021/nl504170d
Nano Lett. 2015, 15, 1627−1634

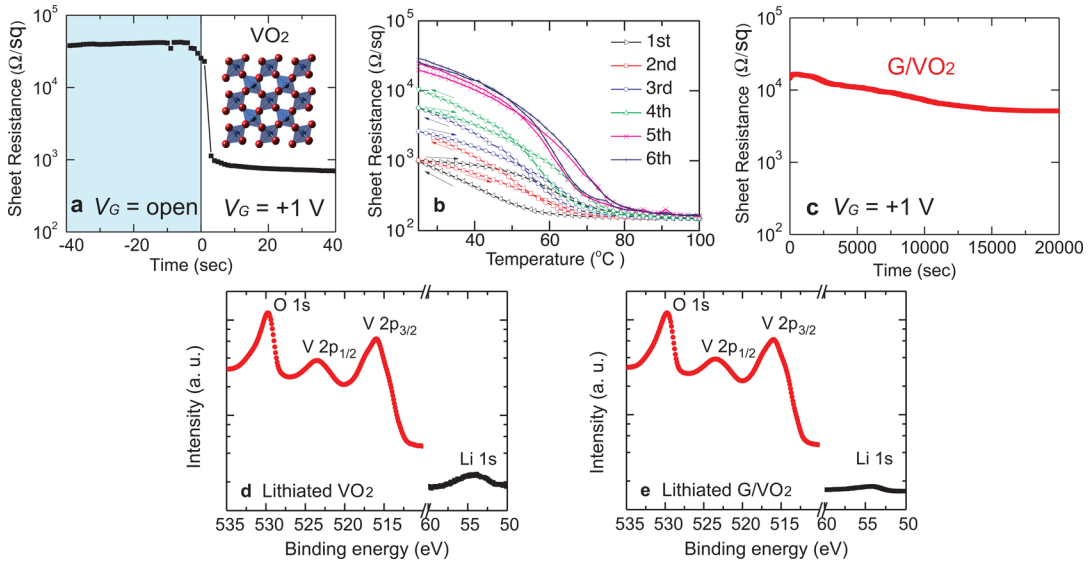

Figure 6. (a) Evolution of channel sheet resistance of bare VO_2 device during lithium intercalation process. Initially no gate voltage is applied, and the channel resistance remains constant. At t = 0 s, a gate voltage of +1 V is applied and the channel resistance drops sharply. The inset shows the oxygen octahedra and open channels in the monoclinic phase of VO_2 viewed along the a axis. The red and blue spheres correspond to oxygen and vanadium atoms, respectively. (b) Delithiation process after bare VO_2 is intercalated with lithium. The resistance slowly reverses back close to original value after a few thermal cycles. (c) Lithium intercalation of graphene-coated VO_2. X-ray photoelectron spectra of (d) bare VO_2 and (e) graphene-coated samples after being lithiated under +1 V for 1 h. The peak ratios of V 2p to Li 1s show that lithium has been intercalated into the samples with different atom percentage.

Electrochemical reactions create oxygen defects that act as electron donors to VO_2 by the defect equlibria $O_O^X \leftrightarrow V_O^{2+} + 2e + 1/2\ O_2$ (Kröger−Vink notation) in ionic liquids, and graphene interfaces allow us to investigate its protection capacity to more reactive and smaller electrochemical species such as lithium ions. We performed lithium intercalation experiments on both bare and graphene-coated VO_2 devices using lithium perchlorate ($LiClO_4$) dissolved in propylene carbonate as electrolyte and lithium metal as the gate electrode. Figure 6a shows the evolution of channel resistance of a bare VO_2 device under 1 V gate bias. Initially the circuit between gate and VO_2 is open so that no electric current can flow through and the channel conductance remains unchanged. At t = 0 s, when a gate voltage of +1 V is applied, the channel resistance drops instantaneously by about 50 times and becomes constant. The half reaction that happens on the lithium metal is $Li \rightleftharpoons Li^+ + e$. The Li^+ ions are transported through the electrolyte and become intercalated into VO_2, while the electrons are doped into VO_2 through the external circuit. The electrons doped by Li intercalation suppress the metal−insulator transition in VO_2 in a similar way as by oxygen vacancies as shown in Figure 6b. The resistance of the insulating state is reduced while the effective transition temperature as determined by the peak of (d ln R)/dT curves is lowered. It is also interesting to notice that the lithium ions can be deintercalated from VO_2 matrix after a few thermal cycles as indicated by Figure 6b. In the deintercalation process, both the lithium ion and electron diffuse out from VO_2 matrix, leading to a reversible modification of VO_2 conductance. An interesting observation is that the conductance modulation happens at a time scale of few seconds, much faster than what is seen in typical ionic liquid gating experiments. One reason is that the reactivity of Li metal provides a large driving force for the reactions to happen. In addition, VO_2 has a distorted rutile structure, where there are open channels along the a axis of the monoclinic phase (c axis of the rutile phase) as shown in the inset of Figure 6a. It has been observed in rutile TiO_2 that ions such as H^+ and Li^+ can diffuse along c axis at speeds orders of magnitude larger than the perpendicular crystal axes.[36,37] Similarly, the ions may transport in VO_2 in a quasi-1D fashion, leading to fast lithium intercalation and conductance modulation.

To study the effect of graphene on the lithium intercalation process in VO_2, identical experiments were performed on graphene-coated devices and the results are shown in Figure 6c. It is striking that the rate of lithium intercalation is significantly retarded by the graphene interlayer for well over 5 h. We see a very slow drop of resistance that indicates that intercalation occurs but at an extremely slow rate that is more than 5 orders of magnitude slower than the bare VO_2. It is presumably from transporting a trace amount of lithium ions through atomic or line defects in the graphene sheet. Consequently, the crystalline honeycomb structure composed of carbon atoms in graphene works successfully as a protective layer for reactive lithium ions with the size of ∼0.090 nm.[12] X-ray photoelectron spectroscopy confirmed the different lithiation behavior of bare VO_2 and graphene-coated VO_2 devices. Both types of devices were gated using lithium electrolyte at +1 V for 1 h and cleaned with acetone, isopropanol, DI water, and blow-dried with N_2 before XPS characterization. First, we observed a strong lithium peak along with the vanadium peak as shown in Figure 6d, supporting that active lithium intercalation reaction takes place in a bare VO_2 device. The lithium to vanadium ratio is estimated to be 1:4 from peak intensity and relative sensitivity factors (RSF) in the spectra for bare VO_2 samples. Notice that the peak intensity of Li 1s is much smaller than V 2p, which is because lithium has a very small scattering cross-section and therefore low RSF value (0.0568 for Li 1s and 6.37 for V 2p3/2 for the instrument). In addition, the lithium 1s peak position is at ∼54.5 eV, corresponding to Li−O bond, which suggests lithium is bonded to oxygen in VO_2 matrix.[38] However, the lithium-to-vanadium ratio is less than 1:16 on the graphene-

DOI: 10.1021/nl504170d
Nano Lett. 2015, 15, 1627−1634

coated VO_2 device, (Figure 6e). This result is consistent with the retarded resistance response from inhibition of lithium intercalation in the presence of graphene layer onto VO_2.

We then confirmed that the ability of graphene to impede electron-doping can be extended to protons that are even smaller than lithium ions. Previous studies have investigated the doping effect of protons in VO_2 and have found hydrogenation could fully stabilize the metallic phase of VO_2 at room temperature.[39] By using DI water as gating medium and injecting protons by applying a gate voltage of +2 V, we studied the behavior of gating of bare VO_2 and graphene−VO_2 devices. At +2 V bias, the resistance slightly drops as protons dope VO_2 as shown in Figure 7. Although the channel response is slowed

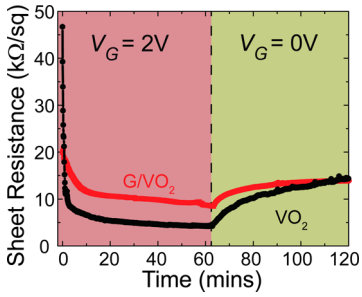

Figure 7. Electrochemical gating using DI water as electrolyte on VO_2 and graphene−VO_2 device. The channel resistance changes in a slow and hysteretic way under a constant bias of +2 and 0 V in both cases.

down by a few times than unprotected VO_2, the suppression of proton transport is much less than that of lithium ion transport, indicating that graphene imposes a smaller energy barrier for proton than lithium ion.[16,40] After the gate voltage is switched to 0 V, the resistance value increases but does not fully recover to its original value, showing typical hysteretic nonvolatile characteristics. Noting that the channel resistance of bare VO_2 device changes by a few times within just 1 min, we can conclude that such process occurs at a much slower rate with graphene interlayer.

In summary, our results clearly demonstrate that a monolayer of graphene can successfully form a diffusion barrier for ions of a wide size ranging from ionic liquid cations to protons in solution and enable controlling onset of emergent conduction at a prototypical correlated oxide interface. Such interfaces can be valuable in understanding response of field effect devices used to probe electronic phase diagrams of complex systems and the onset of emergent properties at interfaces driven by compositional instability. From an application perspective, electrolyte gating utilizing the electrochemical reactions has recently enabled artificial neural circuits that mimic the synaptic activities in biological brains.[41] Graphene-coated devices that have different channel response dynamics could be used to simulate different types of biological synaptic processes within the same circuit as an example. The ion selectivity of graphene combined with channel conductance modulation could be of relevance to the realization of artificial ion channels as well. The results also motivate future directions for research on localized functionalization of complex oxide semiconductor surfaces by using graphene or other two-dimensional materials.

Methods. Vanadium dioxide thin films were grown on *c*-plane sapphire by magnetron sputtering from a V_2O_5 target in pure Ar atmosphere. Before the deposition, the substrates was cleaned by acetone, isopropanol, and DI water and then blow-dried in N_2. The deposition pressure and substrate temperature were kept constant at 4 mTorr and 550 °C. The films are epitaxial on sapphire as confirmed by X-ray diffraction. The film thickness is approximately 100 nm. The VO_2 thin films were patterned by photolithography and reactive ion etching in a CF_4/Ar gas mixture under 100 W forward plasma power. Ti(15 nm)/Au(100 nm) contact were deposited by e-beam evaporation under a pressure of $\sim 10^{-6}$ Torr and patterned by a lift-off process. The fabricated devices have various dimensions. In the gating experiments, devices with the size of 2 mm (length) × 0.4 mm (width) were used.

Graphene was synthesized by chemical vapor deposition (CVD) on 25 μm thick copper foil (99.8%, Alfa Aesar, Ward Hill, MA). The copper foil was inserted into a quartz tube and heated to 1000 °C under H_2 flow of 10 sccm at 300 mTorr. After annealing for 30 min, a gas mixture of 20 sccm CH_4 and 10 sccm H_2 at 750 mTorr was introduced for 20 min to grow grapheme on copper foil substrate. Fast cooling to room temperature was followed with CH_4 flow of 20 and 10 sccm H_2 under a pressure of 750 mTorr. As-prepared graphene on copper foil was spin-coated with poly(methyl methacrylate) (PMMA, 950 A9, Microchem) for facilitating graphene transfer onto the VO_2 device. Back-side graphene was removed by mild oxygen plasma etching. Copper foil was etched by floating PMMA/grapheme/copper foil films onto ammonium persulfate solution (5 g in 100 mL of deionized water) for more than 4 h. Graphene films were rinsed several times by floating onto clean water. Then, they were lifted out with VO_2 devices and dried under vacuum in a desiccator to promote good contact between graphene and the device. Finally, PMMA layer was removed by immersing in acetone several times to provide clean graphene surface. The entire device is covered by graphene.

Electrical characterization was performed using a Keithley 2635A source meter with samples placed on a temperature-controllable chuck. Gate bias was applied with a Keithley 230 voltage supply. In electrolyte gating experiments, two tungsten probes are placed on source and drain electrode with hard contact to the electrodes. For graphene-coated devices, graphene is scratched by the probes in order to form direct contact between the probe and gold source/drain electrodes. In ionic liquid gating experiment, a droplet of IL was dispersed onto the channel while a gold-coated probe is inserted into the IL as the gate electrode. The whole system is sealed in dry N_2 atmosphere during measurements and the ionic liquid is baked at 120 °C beforehand. For H^+ and Li^+ intercalation experiments, DI water and saturated lithium perchlorate in propylene carbonate were used as gating medium, respectively. A probe and a Li metal were used as the gate electrode in the H^+ and Li^+ intercalation, respectively. X-ray photoelectron spectroscopy (XPS) characterization was conducted by a K-Alpha Thermo Scientific XPS system with the data collection area of 200 μm in diameter. Samples were carefully cleaned by acetone, isopropanol, and DI water and then dried by N_2 before measuring the XPS spectra. Raman spectra of various devices were acquired by scanning confocal Raman spectroscopy (WitTec) with a 532 nm laser excitation (1.1 mW).

■ ASSOCIATED CONTENT

Supporting Information

Additional information and figures on AFM, SEM, and electrical. Detailed calculations considering effects of graphene screening, air gap, and pinholes. This material is available free of charge via the Internet at http://pubs.acs.org.

DOI: 10.1021/nl504170d
Nano Lett. 2015, 15, 1627−1634

AUTHOR INFORMATION

Corresponding Author

*E-mail: youzhou@seas.harvard.edu.

Present Address

(J.S.) Department of Materials Science and Engineering, Rensselaer Polytechnic Institute.

Author Contributions

Y.Z. and J.P. contributed equally to this work.

Notes

The authors declare no competing financial interest.

ACKNOWLEDGMENTS

This work was supported by the National Science Foundation, National Academy of Sciences, NSF (DMR-1310266), the Harvard Materials Research Science and Engineering Center (DMR-0820484), and Amore-Pacific.

REFERENCES

(1) Ahn, C. H.; Bhattacharya, A.; Di Ventra, M.; Eckstein, J. N.; Frisbie, C. D.; Gershenson, M. E.; Goldman, A. M.; Inoue, I. H.; Mannhart, J.; Millis, A. J.; Morpurgo, A. F.; Natelson, D.; Triscone, J.-M. *Rev. Mod. Phys.* **2006**, *78* (4), 1185−1212.

(2) Zhou, Y.; Ramanathan, S. *Crit. Rev. Solid State Mater. Sci.* **2013**, *38* (4), 286−317.

(3) Fujimoto, T.; Awaga, K. *Phys. Chem. Chem. Phys.* **2013**, *15* (23), 8983−9006.

(4) Ueno, K.; Nakamura, S.; Shimotani, H.; Yuan, H. T.; Kimura, N.; Nojima, T.; Aoki, H.; Iwasa, Y.; Kawasaki, M. *Nat. Nanotechnol.* **2011**, *6* (7), 408−412.

(5) Lee, Y.; Clement, C.; Hellerstedt, J.; Kinney, J.; Kinnischtzke, L.; Leng, X.; Snyder, S. D.; Goldman, A. M. *Phys. Rev. Lett.* **2011**, *106* (13), 136809.

(6) Yamada, Y.; Ueno, K.; Fukumura, T.; Yuan, H. T.; Shimotani, H.; Iwasa, Y.; Gu, L.; Tsukimoto, S.; Ikuhara, Y.; Kawasaki, M. *Science* **2011**, *332* (6033), 1065−1067.

(7) Yang, Z.; Zhou, Y.; Ramanathan, S. *J. Appl. Phys.* **2012**, *111*, 014506.

(8) Buzzeo, M. C.; Evans, R. G.; Compton, R. G. *ChemPhysChem* **2004**, *5* (8), 1106−1120.

(9) Lewandowski, A.; Galiński, M. *J. Phys. Chem. Solids* **2004**, *65* (2−3), 281−286.

(10) Ohno, H. *Electrochemical Aspects of Ionic Liquids*; John Wiley & Sons: New York, 2011.

(11) Garaj, S.; Hubbard, W.; Reina, A.; Kong, J.; Branton, D.; Golovchenko, J. A. *Nature* **2010**, *467* (7312), 190−193.

(12) Berry, V. *Carbon* **2013**, *62* (0), 1−10.

(13) Yuk, J. M.; Park, J.; Ercius, P.; Kim, K.; Hellebusch, D. J.; Crommie, M. F.; Lee, J. Y.; Zettl, A.; Alivisatos, A. P. *Science* **2012**, *336* (6077), 61−64.

(14) Koenig, S. P.; Wang, L.; Pellegrino, J.; Bunch, J. S. *Nat. Nanotechnol.* **2012**, *7* (11), 728−732.

(15) Cohen-Tanugi, D.; Grossman, J. C. *Nano Lett.* **2012**, *12* (7), 3602−3608.

(16) Wang, W. L.; Kaxiras, E. *New J. Phys.* **2010**, *12* (12), 125012.

(17) Zhou, Y.; Ramanathan, S. *J. Appl. Phys.* **2012**, *111*, 084508.

(18) Ji, H.; Wei, J.; Natelson, D. *Nano Lett.* **2012**, *12* (6), 2988−2992.

(19) Nakano, M.; Shibuya, K.; Okuyama, D.; Hatano, T.; Ono, S.; Kawasaki, M.; Iwasa, Y.; Tokura, Y. *Nature* **2012**, *487* (7408), 459−462.

(20) Liu, K.; Fu, D.; Cao, J.; Suh, J.; Wang, K. X.; Cheng, C.; Ogletree, D. F.; Guo, H.; Sengupta, S.; Khan, A.; Yeung, C. W.; Salahuddin, S.; Deshmukh, M. M.; Wu, J. *Nano Lett.* **2012**, *12* (12), 6272−6277.

(21) Jeong, J.; Aetukuri, N.; Graf, T.; Schladt, T. D.; Samant, M. G.; Parkin, S. S. P. *Science* **2013**, *339* (6126), 1402−1405.

(22) Sim, J. S.; Zhou, Y.; Ramanathan, S. *Nanoscale* **2012**, *4*, 7056.

(23) Giovannetti, G.; Khomyakov, P.; Brocks, G.; Karpan, V.; Van den Brink, J.; Kelly, P. *Phys. Rev. Lett.* **2008**, *101* (2), 026803.

(24) Sohn, A.; Kim, H.; Kim, D.-W.; Ko, C.; Ramanathan, S.; Park, J.; Seo, G.; Kim, B.-J.; Shin, J.-H.; Kim, H.-T. *Appl. Phys. Lett.* **2012**, *101*, 191605.

(25) Visscher, P.; Falicov, L. *Phys. Rev. B* **1971**, *3* (8), 2541−2547.

(26) Guinea, F. *Phys. Rev. B* **2007**, *75* (23), 235433.

(27) Miyazaki, H.; Odaka, S.; Sato, T.; Tanaka, S.; Goto, H.; Kanda, A.; Tsukagoshi, K.; Ootuka, Y.; Aoyagi, Y. *Appl. Phys. Express* **2008**, *1* (3), 034007.

(28) Kosuke, N.; Tomonori, N.; Koji, K.; Akira, T. *Jpn. J. Appl. Phys.* **2010**, *49* (5R), 051304.

(29) Chen, F.; Qing, Q.; Xia, J.; Li, J.; Tao, N. *J. Am. Chem. Soc.* **2009**, *131* (29), 9908−9909.

(30) Schilbe, P. *Phys. B: Condens. Matter* **2002**, *316-317* (0), 600−602.

(31) Jones, A. C.; Berweger, S.; Wei, J.; Cobden, D.; Raschke, M. B. *Nano Lett.* **2010**, *10* (5), 1574−1581.

(32) Ferrari, A. C.; Meyer, J. C.; Scardaci, V.; Casiraghi, C.; Lazzeri, M.; Mauri, F.; Piscanec, S.; Jiang, D.; Novoselov, K. S.; Roth, S.; Geim, A. K. *Phys. Rev. Lett.* **2006**, *97* (18), 187401.

(33) Gupta, A.; Chen, G.; Joshi, P.; Tadigadapa, S.; Eklund. *Nano Lett.* **2006**, *6* (12), 2667−2673.

(34) Mills, D. L.; Maradudin, A. A.; Burstein, E. *Ann. Phys.* **1970**, *56* (2), 504−555.

(35) Ponosov, Y. S.; Streltsov, S. V. *Phys. Rev. B* **2012**, *86* (4), 045138.

(36) Johnson, O. W. *Phys. Rev.* **1964**, *136* (1A), A284−A290.

(37) Kingsbury, P. I.; Ohlsen, W. D.; Johnson, O. W. *Phys. Rev.* **1968**, *175* (3), 1099−1101.

(38) Suo, L.; Hu, Y.-S.; Li, H.; Armand, M.; Chen, L. *Nat. Commun.* **2013**, *4*, 1481.

(39) Wei, J.; Ji, H.; Guo, W.; Nevidomskyy, A. H.; Natelson, D. *Nat. Nanotechnol.* **2012**, *7* (6), 357−362.

(40) Das, D.; Kim, S.; Lee, K.-R.; Singh, A. K. *Phys. Chem. Chem. Phys.* **2013**, *15* (36), 15128−15134.

(41) Ha, S. D.; Shi, J.; Meroz, Y.; Mahadevan, L.; Ramanathan, S. *Phys. Rev. Appl.* **2014**, *2* (6), 064003.

DOI: 10.1021/nl504170d
Nano Lett. 2015, 15, 1627−1634